Two-Dimensional Visualization of Growth and Burst of the Edge-Localized Filaments in KSTAR *H*-Mode Plasmas

G. S. Yun,[1] W. Lee,[1] M. J. Choi,[1] J. Lee,[1] H. K. Park,[1] B. Tobias,[2] C. W. Domier,[3] N. C. Luhmann, Jr.,[3] A. J. H. Donné,[4] J. H. Lee,[5] and KSTAR Team

[1]*POSTECH, Pohang, Republic of Korea*
[2]*Princeton Plasma Physics Laboratory, Princeton, New Jersey, USA*
[3]*University of California, Davis, California, USA*
[4]*FOM Institute for Plasma Physics Rijnhuizen, Nieuwegein, The Netherlands*
[5]*National Fusion Research Institute, Daejeon, Republic of Korea*

(Received 22 March 2011; published 22 July 2011)

The filamentary nature and dynamics of edge-localized modes (ELMs) in the KSTAR high-confinement mode plasmas have been visualized in 2D via electron cyclotron emission imaging. The ELM filaments rotating with a net poloidal velocity are observed to evolve in three distinctive stages: initial linear growth, interim quasisteady state, and final crash. The crash is initiated by a narrow fingerlike perturbation growing radially from a poloidally elongated filament. The filament bursts through this finger, leading to fast and collective heat convection from the edge region into the scrape-off layer, i.e., ELM crash.

DOI: 10.1103/PhysRevLett.107.045004 PACS numbers: 52.30.Cv, 52.35.Py, 52.35.Vd, 52.55.−s

Edge-localized modes (ELMs) [1] are a class of semiperiodic relaxation events of the excess pressure built up in the edge transport barrier region (also called *pedestal*) of high-confinement mode (*H*-mode) toroidal plasmas [2]. Understanding and control of ELMs are considered essential for the *H*-mode operation such as impurity transport and safety of the first wall of future magnetic fusion devices [3]. The generally accepted physical mechanism for the onset of ELMs involves two competing magnetohydrodynamic instabilities arising in the pedestal [4]: the ballooning mode driven by the steep pressure gradient and the kink-type instability called the peeling mode due to the edge current close to the last closed flux surface (LCFS). The coupled peeling-ballooning stability limits are in good agreement with the observed thresholds for the onset of ELMs [5].

The filamentary nature of the ELM perturbations has recently been observed in a number of tokamaks including MAST [6,7], ASDEX-U [8,9], JET [10], DIII-D [11], NSTX [12], and C-Mod [13]. These studies revealed that the ELMs are filamentary perturbations of positive density formed along the local field lines close to the LCFS, and the filaments suddenly detach or burst at different times from the pedestal and expand radially during the ELM crash phase. The particles and heat carried by the expanding filaments were found to be significantly less than the total loss during the ELM crash, suggesting that the bursts of filaments induced confinement degradation for an extended region of the pedestal. Despite significant improvements in understanding of the ELM filaments, the majority of the previous observations were confined to the filaments outside the LCFS (i.e., in the scrape-off layer) after or during the burst. Because of the lack of detailed observations in the pedestal region prior to the burst, except for a few important 2D imaging measurements [11,14], many important features of the ELM evolution remain unclear, such as the nonuniformity and nonlinearity of the filament growth, the trigger mechanism for the sudden burst of the filaments, the spatial extent of the burst zone, and the source of particles to account for the filament growth.

In the 2010 KSTAR campaign, the entire temporal and spatial evolution process of the filamentary ELM structures has been captured in 2D using an electron cyclotron emission imaging (ECEI) system [15]. The ECEI is a 2D imaging diagnostic based on the established radiometry for the local measurements of electron cyclotron emission (ECE) intensity (T_*), which is linearly proportional to the electron temperature (T_e) in the case of optically thick plasmas [16]. Previous generation ECEI systems have played a critical role for advancing our understanding of the core MHD physics such as sawteeth [17], tearing modes [18], Alfvén eigenmodes [19], and also edge MHD phenomena [14]. The KSTAR ECEI system has independent dual detector arrays capable of simultaneous measurements of low-field side (LFS) and high-field side (HFS) in the same poloidal cross section, providing an excellent opportunity to address any correlation between the core and edge dynamics such as "sawtooth triggered ELMs." Each detector array provides 24 (vertical) $\times$ 8 (radial) = 192 local T_* measurements, covering a rectangular region of 30–90 cm height and 10–15 cm width with spatial resolution $\sim$1–2 cm and time resolution ~ 1 μs.

Detailed observations of the evolving ELM filaments inside the LCFS using the 2D images of relative T_* fluctuations ($\delta T_*/\bar{T}_*$, where $\delta T_* = T_* - \bar{T}_*$ and $\bar{T}_*$ is a time average) [17] and new insights on the ELM dynamics are discussed in this Letter. Specifically, three distinct evolution phases have been identified and are described in detail: (1) the initial growth of the ELM filaments, (2) the interim

quasisteady state of saturated filaments, and (3) the final crash phase characterized by a poloidal elongation of filaments, development of a fingerlike structure bulging outward and rapid crash through this finger.

Figure 1(a) shows the time traces of the Balmer alpha (D_α) emission, core and edge ECEI signals, and the line-averaged electron density ($n_{e,l}$) for a typical H-mode discharge obtained during the 2010 KSTAR campaign. The plasma was a D-shaped deuterium discharge heated by cocurrent neutral beam ~1 MW and perpendicular electron cyclotron resonance wave (110 GHz) ~ 250 kW with magnetic field $B_0 = 1.96$ T, plasma current $I_p = 600$ kA, core $T_e \sim 1$ keV, and $n_{e,l} \sim 3.5 \times 10^{19}$ m^{-3}. The H-mode transition as indicated by a large drop in D_α at $t \sim 1.23$ s was slow due to the marginal heating power compared to typical transitions observed in other tokamaks. Nonetheless, the formation of pedestal was clearly observed by a charge exchange spectroscopy (CES) system [20], which measured a steep ion temperature (T_i) gradient from ~750 to ~200 eV in the narrow edge region ~5 cm. Following the transition, a typical sequence of ELM behaviors was observed, i.e., initially small-amplitude ELMs, quiescent period, and large-amplitude ELMs. The latter is presumably type-I ELMs although an accurate classification is only feasible when the heating power scanning and stability analysis will become available in the next KSTAR campaign.

Figure 1(b) (center) illustrates the equilibrium magnetic flux surfaces reconstructed by the EFIT algorithm [21]

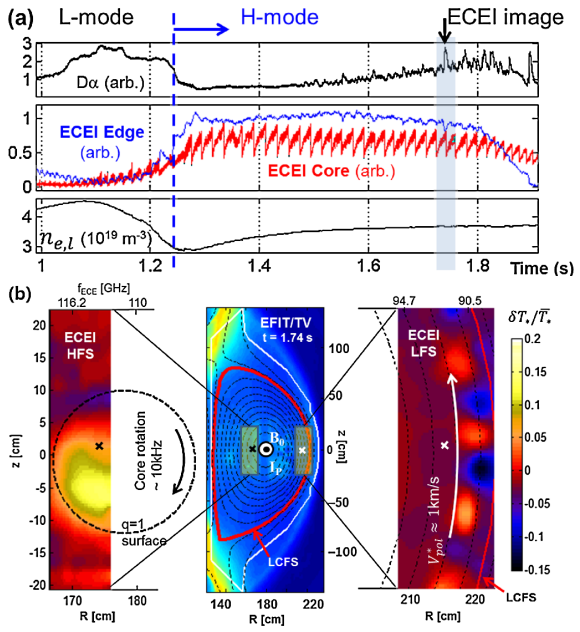

FIG. 1 (color online). (a) Time evolution of D_α emission, core and edge ECEI signals, and $n_{e,l}$ for ELMy H-mode plasma (shot no. 4362). (b) ECEI snapshot showing the core $m/n = 1/1$ internal kink (left) and the edge filaments (right). The cross marks are the approximate positions of the two ECEI channels. The middle figure depicts EFIT reconstructed flux surfaces overlaid on top of a fast visible camera image. The directions of B_0 and I_p are both out of the plane.

during the steady H-mode state. Note that the local field lines on the flux surfaces are right handed since both B_0 and I_p are in the same direction (out of the plane in the figure). The corresponding LFS ECEI image (right) clearly demonstrates the filamentary structure at the edge and the HFS image (left) illustrates a displaced hot core due to the $m/n = 1/1$ internal kink instability at the same time. Interestingly, the apparent poloidal rotation is reversed from the core (clockwise) to the edge (counterclockwise), which demonstrates the existence of a strong flow shear. In the edge, the counterclockwise rotation of the filaments implies a net poloidal flow $V_{\rm pol} \sim +4$ km/s according to the relation $V^*_{\rm pol} = V_{\rm pol} - V_{\rm tor}\tan(\alpha)$ using the observed apparent velocity $V^*_{\rm pol} \sim +1$ km/s, the toroidal plasma rotation $V_{\rm tor} \sim +50$ km/s from CES, and the pitch angle of the magnetic field lines $\alpha \sim +3.5°$ (the signs are with respect to the direction of the magnetic axis). In the core, $V_{\rm tor} \sim +100$ km/s is dominant and consistent with the observed clockwise rotation of the $m/n = 1/1$ mode ~10 kHz. Note that the LCFS (and other flux surfaces) drawn in the LFS image should be taken as an approximate visual aid due to the uncertainties (up to ~1 cm) both in the EFIT reconstruction and the radial coordinates (R) of the ECEI channels. The latter is estimated from the cold resonance condition of the individual channel frequencies $f_{\rm ECE} \propto B \propto 1/R$, ignoring the relativistic shift of the resonant ECE frequency [16], the radial variation of poloidal magnetic field strength, and instrumental errors.

It should be noted that the major portion of the LFS image inside the LCFS can be treated as a local measurement since the pedestal region will be optically thick or gray (i.e., optical depth $\tau \gtrsim 1$) assuming $T_e =$ 500–200 eV and $n_e = 2$–0.2×10^{19} m^{-3} profiles from the pedestal top to the LCFS. In particular, the clear contrast of the filaments, which are presumably regions of a higher n_e and/or T_e compared to the background plasma in the same flux zone inside the LCFS [7,11,22], is a good indication of the localized measurement [14]. Thus, the observed filamentary structures are real and not an instrumental artifact although the accurate interpretation of the ECE intensity (T_*) inside the filaments is not straightforward. The latter point can be understood by considering n_e variation from 0.3 to 0.6×10^{19} m^{-3} at constant $T_e =$ 300 eV as an example, which can cause an ~10% increase in T_* according to the relations $\tau \propto T_e n_e$ for the second harmonic extraordinary ECE [16] and $T_* \sim T_e(1 - e^{-\tau})/(1 - re^{-\tau})$ [23] with a nominal wall reflection coefficient $r \sim 0.8$. The interpretation of the ECE from further outside the LCFS has to be undertaken with extreme care.

Two different types of ELM crashes have been identified through the time traces of the D_α and edge ECEI signals (one at the pedestal and the other at the filament zone) as illustrated in Fig. 2(a), and the corresponding images of the crash moment are compared in Fig. 2(b). The small crash events corresponding to the semiperiodic (~ 2 ms) small bumps in the D_α trace are observed as a single burst of

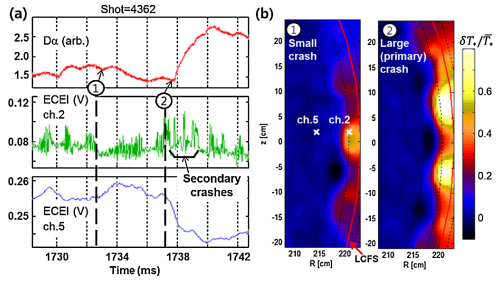

FIG. 2 (color online). (a) Detailed time traces of D_α and ECEI signals from the filament zone (ch.2) and near the pedestal top (ch.5). (b) ECEI images of small and large ELM crashes.

one ELM filament in the ECEI view. The pedestal ECE intensity shows no significant change during these small crashes. On the other hand, the large crash events involve a sharp increase in the D_α signal and a significant drop ($\sim 5\%$–10%) of the pedestal ECE intensity, implying loss of the pedestal confinement. Within the rise time of the D_α signal ($\sim$ a few ms), the large crash generally consists of multiple filament bursts separated by several 100 μs, which is similar to the phenomenology of the primary and secondary filaments studied in NSTX and C-Mod [12,13].

The evolution of the observed ELM filaments typically consists of three distinctive stages: initial growth, quasisteady state, and crash phase. In the first stage during the intercrash period, multiple filamentary structures emerge simultaneously near the LCFS and grow to a saturated state in a short time scale (~ 300 μs) as shown in Fig. 3. The filamentary perturbation structure is conspicuous with the high poloidal mode number $m \sim 40$ estimated from the number of filaments within the ECEI view along the reconstructed flux surface (see the perturbed flux surface models in Fig. 4). The corresponding toroidal mode number would be $n \sim 6$ for the edge safety factor

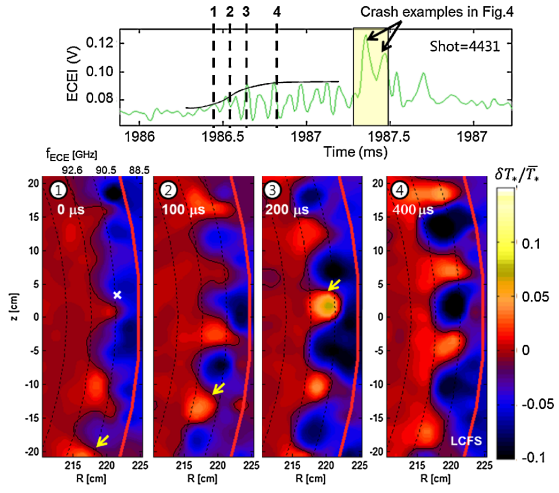

FIG. 3 (color online). Simultaneous emergence and growth of multiple ELM filaments (shot no. 4431). Solid curves are contour lines of the same $\delta T_*/\bar{T}_*$ value representing the approximate boundary of the filaments. The arrows follow the same filament illustrating the counterclockwise rotation.

$q = m/n \sim 6$ estimated from the LCFS geometry and I_p, suggesting that the observed perturbation may be the peeling-ballooning mode instability [4]. The individual filaments grow in amplitude and extend radially outward across flux surfaces on the average (compare frames 1–4 in Fig. 3) with substantial fluctuations of both the amplitude and radial extent, which may suggest toroidally nonuniform growth or temporal variation of the toroidally uniform filaments due to the marginal stability. The average growth rate estimated by the integrated ECE amplitude of the filament regions (defined by an arbitrary intensity contour level) is semiexponential, implying that the instability responsible for the filament growth, presumably the peeling-ballooning mode [4], is in a linear state. The apparent poloidal rotation of the filaments $V^*_{\rm pol}$ is counterclockwise from the moment of birth as indicated by the arrows in Fig. 3. Cases with $V^*_{\rm pol} \leq 0$ were rarely observed, which may imply a critical $V_{\rm pol}$ (or radial electrical field E_r [1,24]) for the onset of the linear instability. In some cases, $V^*_{\rm pol}$ was intermittent instead of being continuous, and the cause of this intermittency is unknown at this point.

The interim saturated state (see frame 4 of Fig. 3) typically persists for $\sim$100 μs. The filaments do not grow on

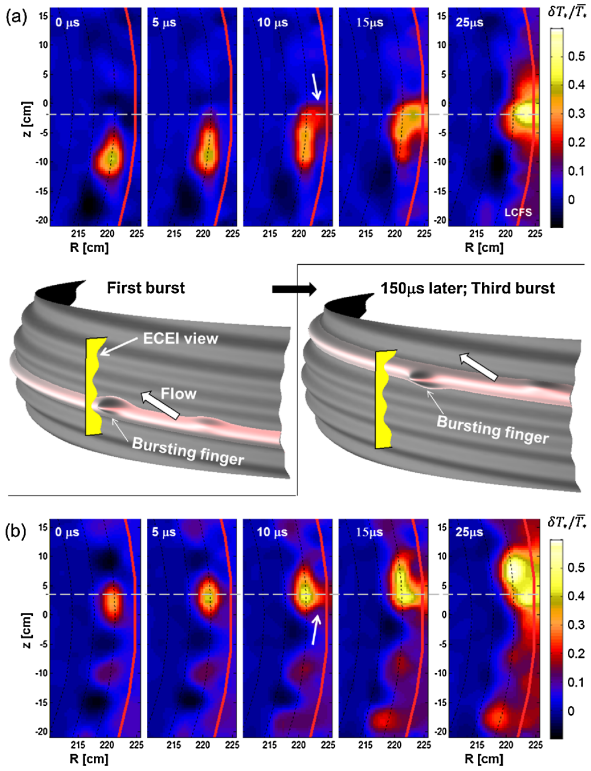

FIG. 4 (color online). Multiple bursts of the same filament in a large ELM crash event. (a) First in the series of four bursts. Bottom left sketch depicts the flux surface with the filamentary perturbations and the burst zone entering the ECEI view. The white box arrow indicates the flow velocity of the filaments. (b) Third burst of the same filament, 150 μs later. Top right sketch is the corresponding model. In each example, the bursting filament develops a narrow fingerlike structure bulging outward.

the average during this stage although the size and amplitude of individual filaments still fluctuate. The quasistability and the large filament size (~ 5 cm) comparable to the pedestal width suggest that the initial linear instability has evolved into a metastable nonlinear phase [25] although the underlying stabilization mechanism is not clear. The observed large variation in the duration of the saturated states from being almost absent to several 100 μs also indicates the metastability of this stage under the influence of random perturbations. A very short transient period of $\lesssim 50$ μs has been frequently observed between the saturated state and the final crash phase. The filaments almost disappear from the ECEI view and then reemerge with a reduced number of filaments (or larger distance between filaments). The abrupt change in the poloidal mode number may be important for the crash trigger mechanism, which needs further investigation.

The crash phase is much more complex due to the nonlinear and nonaxisymmetric nature of the crash dynamics. The detailed sequence of a typical crash process is described by two examples of filament bursts in Fig. 4. These examples are actually the first and third bursts in a series of four bursts of the same filament occurring in $\sim$200 μs time period, which is much longer than the parallel transport time scale of the thermal electrons once around the torus (~ 1 μs) and the toroidal Alfvén time scale (~ 1 μs). A phenomenological description of this situation is appended in each example, illustrating the locations of the active burst zone and other burst zones at different times along the moving filamentary perturbations and the position of the fixed ECEI observation window. The crash phase starts with the poloidal elongation of the filaments as shown in the first frame of each example. Note that the elongation is not a result of squeezing since the radial size does not change appreciably. Then, a narrow fingerlike perturbation structure develops at one of the filaments as indicated by the arrow in the third frame of each example. As this finger extends radially and touches the LCFS, the ECE intensity along the finger and outside the LCFS increases rapidly indicating particle-heat flux through the finger. The dominant radial flux, lasting for $\sim$50 μs or less, is localized and convective rather than diffusive, which suggests that the underlying mechanism of the ELM filament burst may be similar to the pressure-driven localized burst and collective heat transport in the sawtooth crashes [17]. Interestingly, the poloidal rotation of the finger is slower compared to the rest of the bursting filament as indicated by the dashed lines in Fig. 4. A magnetic reconnection may be responsible for this slowing-down or braking of the finger as well as the collective heat transport. The finger-initiated crash suggests the toroidal localization of the burst zone, which is also supported by the equally frequent observation of another seemingly different crash pattern characterized by a sudden heat pulse appearing from outside the LCFS and spreading over the entire filament region within $\sim$10 μs.

In summary, the filamentary nature and nonlinear dynamics of ELMs have been studied in 2D using the ECEI system. The ELMs have been found to evolve in three stages: the initial linear phase, the quasisteady state, and the crash phase. The dynamical properties of the ELM filaments such as growth rate, poloidal and toroidal flows, and localized burst through a narrow fingerlike perturbation have been analyzed. The observations presented in this work are in qualitative agreement with the linear predictions of ELMs being strongly localized in the pedestal [4] and the nonlinear predictions of explosive burst of metastable ELM filaments [25]. A phenomenological model of the ELM crash with multiple burst zones has been proposed to explain the crash patterns observed by the ECEI. We emphasize that the ELM crashes in the plasma edge are inherently 3D, nonaxisymmetric, and localized events similar to the sawtooth crashes in the plasma core [17].

We thank Dr. Steve Sabbagh and Dr. Young-Seok Park for providing EFIT results, Mr. Yong-Sun Kim for engineering support during the installation of the ECEI system, and Dr. Patrick Diamond for valuable discussions on the ELM physics. This work was supported by the NRF Korea, the U.S. DOE, and the Association Euratom-FOM.

[1] J. W. Connor, Plasma Phys. Controlled Fusion **40**, 191 (1998).
[2] F. Wagner, Plasma Phys. Controlled Fusion **49**, B1 (2007).
[3] E. J. Doyle *et al.*, Nucl. Fusion **47**, S18 (2007).
[4] P. B. Snyder *et al.*, Phys. Plasmas **9**, 2037 (2002).
[5] P. B. Snyder *et al.*, Plasma Phys. Controlled Fusion **46**, A131 (2004).
[6] A. Kirk *et al.*, Phys. Rev. Lett. **92**, 245002 (2004).
[7] A. Kirk *et al.*, Phys. Rev. Lett. **96**, 185001 (2006).
[8] A. Kirk *et al.*, Plasma Phys. Controlled Fusion **47**, 995 (2005).
[9] A. Schmid *et al.*, Plasma Phys. Controlled Fusion **50**, 045007 (2008).
[10] C. Silva *et al.*, Plasma Phys. Controlled Fusion **51**, 105001 (2009).
[11] J. A. Boedo *et al.*, Phys. Plasmas **12**, 072516 (2005).
[12] R. J. Maqueda, R. Maingi, and NSTX Team, Phys. Plasmas **16**, 056117 (2009).
[13] J. L. Terry *et al.*, J. Nucl. Mater. **363–365**, 994 (2007).
[14] I. G. J. Classen *et al.*, Rev. Sci. Instrum. **81**, 10D929 (2010).
[15] G. S. Yun *et al.*, Rev. Sci. Instrum. **81**, 10D930 (2010).
[16] M. Bornatici *et al.*, Nucl. Fusion **23**, 1153 (1983).
[17] H. K. Park *et al.*, Phys. Rev. Lett. **96**, 195003 (2006).
[18] I. G. J. Classen *et al.*, Phys. Rev. Lett. **98**, 035001 (2007).
[19] B. J. Tobias *et al.*, Phys. Rev. Lett. **106**, 075003 (2011).
[20] W. H. Ko *et al.*, Rev. Sci. Instrum. **81**, 10D740 (2010).
[21] L. Lao *et al.*, Nucl. Fusion **25**, 1611 (1985).
[22] B. Kurzan, H. D. Murmann, and J. Neuhauser, Phys. Rev. Lett. **95**, 145001 (2005).
[23] G. Bekefi, *Radiation Processes in Plasmas* (John Wiley and Sons, Inc., New York, 1966).
[24] K. H. Burrell, Phys. Plasmas **6**, 4418 (1999).
[25] H. R. Wilson and S. C. Cowley, Phys. Rev. Lett. **92**, 175006 (2004).